



# Linkage between Dust Cycle and Loess of the Last Glacial Maximum in Europe

Erik J. Schaffernicht<sup>1</sup>, Patrick Ludwig<sup>2</sup>, and Yaping Shao<sup>1</sup>

<sup>1</sup>Institute for Geophysics and Meteorology, University of Cologne, 50969 Köln, Germany

<sup>2</sup>Institute for Meteorology and Climate Research, Karlsruhe Institute of Technology, 76131 Karlsruhe, Germany

**Correspondence:** Erik J. Schaffernicht (eschaffe@uni-koeln.de)

**Abstract.** This article establishes a linkage between the mineral dust cycle and loess deposits during the Last Glacial Maximum (LGM) in Europe. To this aim, we simulate the LGM dust cycle at high resolution using a regional climate-dust model. The model-simulated dust deposition rates are found to be comparable with the mass accumulation rates of the loess deposits determined from more than 70 sites. In contrast to the present-day prevailing westerlies, winds from northeast, east and southeast (36%) and cyclonic regimes (22%) were found to prevail over central Europe during the LGM. This supports the hypothesis that the recurring east sector winds associated with a high-pressure system over the Eurasian ice sheet (EIS) dominated the dust transport from the EIS margins in eastern and central Europe. The highest dust emission rates in Europe occurred in summer and autumn. Almost all dust was emitted from the zone between the Alps, the Black Sea and the southern EIS margin. Within this zone, the highest emission rates were located near the southernmost EIS margins corresponding to the present-day German-Polish border region. Coherent with the persistent easterlies, westwards running dust plumes resulted in high deposition rates in western Poland, northern Czechia, the Netherlands, the southern North Sea region and on the North German Plain including adjacent regions in central Germany. The agreement between the climate model simulations and the mass accumulation rates of the loess deposits corroborates the proposed LGM dust cycle hypothesis for Europe.

## 1 Introduction

The Last Glacial Maximum (LGM,  $21\,000 \pm 3\,000$  yr ago) is a milestone in the Earth's climate, marking the transition from the Pleistocene to the Holocene (Clark et al., 2009; Hughes et al., 2015). During the LGM, Europe was dustier, colder, windier and less vegetated than today (Újvári et al., 2017). The polar front and the westerlies were located at lower latitudes associated with a significant increase in dryness in central and eastern Europe (COHMAP Members, 1988; Peyron et al., 1998; Florineth and Schlüchter, 2000; Laîné et al., 2009; Heyman et al., 2013; Ludwig et al., 2017). The formation of the Eurasian ice sheet (EIS, Fig. 1 and 2) synchronized with a sea level lowering of between 127.5 m and 135 m (Yokoyama et al., 2000; Clark and Mix, 2002; Clark et al., 2009; Austermann et al., 2013; Lambeck et al., 2014). It led to different regional circulation patterns over Europe (Ludwig et al., 2016). The greenhouse gas concentrations (185 ppmv CO<sub>2</sub>, 360 ppbv CH<sub>4</sub>) were less than half compared to today (Monnin et al., 2001) providing more favorable conditions for C<sub>4</sub> than C<sub>3</sub> plants. This led to more open vegetation (Prentice and Harrison, 2009; Bartlein et al., 2011) such as grassland, steppe, shrub and herbaceous tundra (Kaplan



et al., 2003; Ugan and Byers, 2007; Gasse et al., 2011; Shao et al., 2018). Central and eastern Europe were partly covered by  
26 taiga, cold steppe or montane woodland containing isolated pockets of temperate trees (Willis and van Andel, 2004; Fitzsim-  
mons et al., 2012). Polar deserts characterized the unglaciated areas in England, Belgium, Denmark, Germany, northern France,  
28 western Poland and the Netherlands (Ugan and Byers, 2007). These land surfaces and biome types favored more dust storms  
and transport over Europe (Újvári et al., 2012).

30 Loess as a paleoclimate proxy provides one of the most complete continental records for characterizing climate change and  
evaluating paleoclimate simulations (Singhvi et al., 2001; Haase et al., 2007; Fitzsimmons et al., 2012; Varga et al., 2012).  
32 In Europe, loess covers large areas with major deposits centered around 50°N (Antoine et al., 2009b; Sima et al., 2013).  
However, although numerous European loess sequences date to the LGM, it is not well understood where the dust originated  
34 that contributed to the loess formation (Fitzsimmons et al., 2012; Újvári et al., 2017). There are various hypotheses for the  
potential dust sources, yet they are not fully tested because the dust cycle of the LGM is neither well understood nor quantified.  
36 The use of loess as a proxy for paleoclimate reconstruction is considerably compromised because the linkage between the loess  
deposits and the responsible physical processes is unclear (Újvári et al., 2017). Reliable paleodust modeling is a promising way  
38 to establish this linkage and strengthen the physical basis for paleoclimate reconstructions using loess records. Such attempts  
have been made for example by Antoine et al. (2009b), who analyzed the Nussloch record. They suggested that rapid and  
40 cyclic aeolian deposition due to cyclones played a major role in the European loess formation during the LGM.

However, significant discrepancies exist between the mass accumulation rates (MARs) of aeolian deposits that are estimated  
42 from fieldwork samples and the dust deposition rates calculated by climate model simulations (Újvári et al., 2010): For Europe,  
the global LGM simulations calculate dust deposition rates of less than 100 g m<sup>-2</sup> yr<sup>-1</sup> (Werner, 2002; Mahowald et al., 2006;  
44 Hopcroft et al., 2015; Sudarchikova et al., 2015; Albani et al., 2016). These are substantially smaller than the MARs (on  
average: 800 g m<sup>-2</sup> yr<sup>-1</sup>) that have been reconstructed from more than 70 different loess sites across Europe (Supplementary  
46 Table S1).

For this study, we simulated the aeolian dust cycle in Europe using a LGM-adapted version of the Weather Research and  
48 Forecasting Model coupled with Chemistry (Klose, pers. comm.; Grell et al., 2005; Fast et al., 2006; Kang et al., 2011; Kumar  
et al., 2014; Su and Fung, 2015) referred to as the WRF-Chem-LGM. Along with its climate modeling capacity, the WRF-  
50 Chem-LGM can well represent the dust emission, transport, and deposition processes. This model capacity allows reducing  
the discrepancies between the MARs and the simulation-based calculated dust deposition rates. It enables the establishment of  
52 a linkage between the glacial dust cycle and the loess deposits.

## 2 Data and Methods

54 The WRF-Chem-LGM consists of fully coupled modules for the atmosphere, land surface, and air chemistry. The simulation  
domain encompasses the European continent including western Russia and most of the Mediterranean (Fig. 1) discretized  
56 by a grid spacing of 50 km and 35 atmospheric layers. The domain boundary conditions were 6-hourly updated by using  
the LGM simulation (MPI-LGM) of the Max-Planck-Institute Earth System Model (MPI-ESM; Jungclaus et al., 2012, 2013;



58 Giorgetta et al., 2013; Stevens et al., 2013). To simulate the dust cycle including dust emission, transport and deposition, the  
dust-only mode of the WRF-Chem-LGM was selected. This mode implies the application of the size-resolved University of  
60 Cologne dust emission scheme (Shao, 2004), the Global Ozone Chemistry Aerosol Radiation Transport (GOCART; Chin et al.,  
2000), the dry (Wesely, 1989) and the wet deposition module (Jung et al., 2005).

62 To replace the present-day WRF surface boundary conditions by the LGM conditions, the data sets for the global 1° resolved  
land-sea mask and the topography offset provided by PMIP3 (Paleoclimate Model Intercomparison Project Phase 3; Braconnot  
64 et al., 2012) were interpolated to the 50 km grid (Fig. 1, Supplementary Table S2 and S3). To represent the LGM glaciers and  
land use, the 2° CLIMAP reconstructions (Climate: Long range Investigation, Mapping, and Prediction; Cline et al., 1984)  
66 were also interpolated to the 50 km grid and converted (Ludwig et al., 2017) to the WRF-compatible United States Geologi-  
cal Survey categories (USGS-24) to replace their present-day analogs. The relative vegetation seasonality during the LGM is  
68 assumed to resemble to the present. Based on this uniformitarianism approach, the CLIMAP maximum LGM vegetation cover  
reconstruction (Cline et al., 1984) was weighted using the corresponding monthly fractions of the present-day WRF maximum  
70 vegetation cover and prescribed in the model.

The erodibility at point  $p$  during the LGM is approximated by

$$72 \quad S = \left( \frac{z_{\max} - z}{z_{\max} - z_{\min}} \right)^5 \quad (1)$$

with  $z$  being the LGM terrain height at  $p$  and  $z_{\min}$  ( $z_{\max}$ ) representing the minimal (maximal) height in the  $10^\circ \times 10^\circ$  area  
74 centered around  $p$  (Ginoux et al., 2001). Setting  $S$  to zero where the CLIMAP bare soil fraction reconstruction is less than  
0.5 refines this approximation. The adapted University of Cologne dust emissions scheme takes into account that the erodi-  
76 bility exceeds a lower limit of 0.09 for emission to occur. This suppresses dust sources in areas that had been attributed small  
physically meaningless interpolation-caused erodibility artifacts. The vegetation and snow cover are considered mutually in-  
78 dependent and uniformly distributed within a grid cell, i.e. the erodible area is multiplied by the fractional factor  $(1 - c_{\text{snow}})$  to  
account for snow cover.

80 To simulate the LGM dust cycle with the WRF-Chem-LGM, two downscaling approaches of the MPI-LGM were imple-  
mented: the dynamic downscaling approach and the statistic dynamic downscaling approach. Both emerge from simulations  
82 that base on identically configured numerical schemes representing the atmospheric chemistry and physics in the WRF-Chem-  
LGM. Using dynamic downscaling, a consecutive 30 year simulation (corresponding to more than 10 000 days) was performed.  
84 In contrast, the statistic dynamic downscaling is based on 130 mutually independent episodes each spanning eight days, or a  
total of 1040 days. The episode selection relies on the Circulation Weather Type (CWT) classification (Jones et al., 1993,  
86 2013; Reyers et al., 2014; Ludwig et al., 2016) of the MPI-LGM records into ten classes: Cyclonic, Anticyclonic, North-  
east, East, Southeast, South, Southwest, West, Northwest and North. To compare the prevailing wind directions over Europe  
88 during the Pre-Industrial (PI) and the LGM, the daily mean sea level pressure patterns (interpolated to  $2.5^\circ$  horizontal grid  
spacing) of the MPI-LGM and the MPI-ESM-P simulation for the PI (MPI-PI) were classified for the region centering around  
90 ( $17.5^\circ\text{E}$ ,  $47.5^\circ\text{N}$ ). For records showing rotational and directional CWT patterns, only the directional pattern is counted. By



counting and statistically evaluating the CWTs of all records, a LGM and a PI CWT occurrence frequency distribution is established. The LGM distribution served to reconstruct the LGM dust cycle using statistic dynamic downscaling. It also enabled analyzing the contributions of each wind regime to the dust cycle.

For the statistic dynamic downscaling, we performed 130 WRF-Chem-LGM simulations in total, i.e. 13 simulations for each of the 10 CWT classes. For each of these eight-day spanning simulations, independent consecutive sequences of boundary conditions were chosen out of all MPI-LGM records of the same CWT class. For CWTs with too few sets of distinct consecutive MPI-LGM records of the required CWT, the remaining sets were chosen applying less strict selection criteria (Table 1). For the analysis of all performed episodic simulations, the first two days of each episode are considered as spin-up days and excluded. The reconstruction of quantity  $Q$  using statistic dynamic downscaling is then calculated from the weighted ensemble mean (Reyers et al., 2014):

$$\langle Q \rangle = \sum_i \frac{f_i}{T} \int_T Q(t) dt \quad (2)$$

with  $i$  representing the  $i^{\text{th}}$  CWT,  $f_i$  its occurrence frequency and  $T$  its duration. To evaluate the simulations, the obtained dust deposition rates are compared to more than 70 independent MARs reconstructed from loess sites located in the simulation domain (Supplementary Table S1).

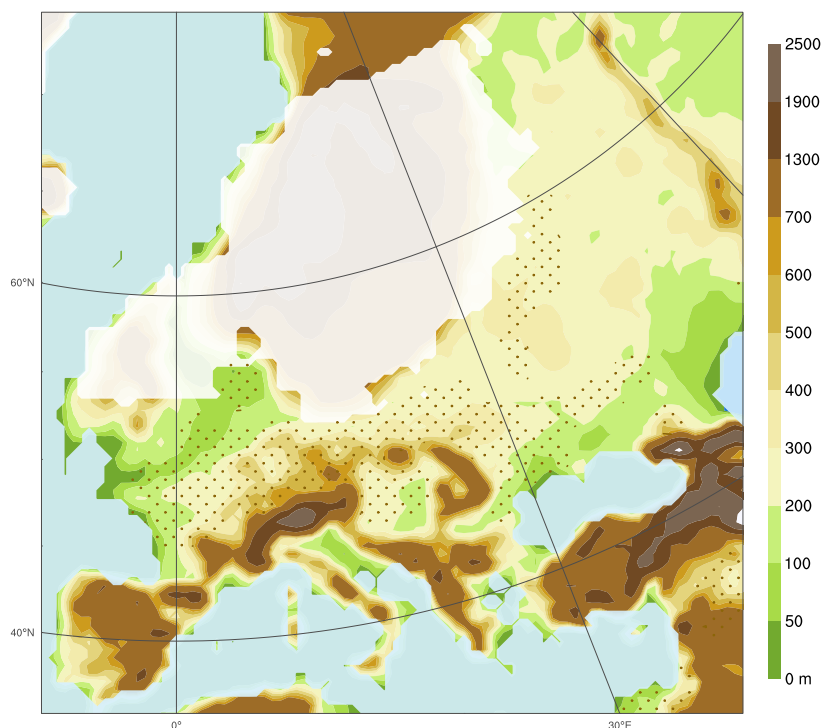


**Figure 1.** Simulation domain showing the applied topography (shaded), the potential dust source areas (dots) and the Eurasian ice sheet extent (white overlay, adapted from Cline et al., 1984) of the Last Glacial Maximum.

**Table 1.** Temporal concept for the episodic eight-day WRF-Chem-LGM simulations performed to reconstruct the LGM dust cycle based on statistic dynamic downscaling. As the MPI-LGM contains for a few CWTs less than 13 separate eight-day record sequences, some of the episodes were driven by a heterogeneous sequence of records. For the selection of the heterogeneous sequences, the CWT-correspondence between main and tracking records is considered of higher priority ( $^{++}$ ) than that between main and spin-up records ( $^{+}$ ).

	Days	Preferences for selecting record series from the MPI-LGM
Spin-up	2	Prefer $^{+}$ series whose spin-up records have the same CWT as the main records
↓		
Main	3	All records forcing the main part of an episode are of the same CWT
↓		
Tracking	3	Prefer $^{++}$ series whose tracking records have the same CWT as the main records



### 3 Results

#### 106 3.1 Dust Cycle Hypothesis

In line with previous modeling (COHMAP Members, 1988; Ludwig et al., 2016) and fieldwork studies (Dietrich and Seelos, 108 2010; Krauß et al., 2016; Römer et al., 2016), we hypothesize that east sector winds (i.e. northeasters, easterlies and southeasters) dominated the mineral dust cycle over central Europe during the LGM (Fig. 2). This hypothesis also implies a linkage of 110 dust sources in central and eastern Europe during the LGM and the loess deposits in Europe. It is suggested here that a greater proportion of all LGM dust deposits in central and eastern Europe comes more from sources in central and eastern Europe 112 than from sources in the Channel. The east sector winds likely contributed substantially to the formation of the European loess belt in central Europe. Among them, the northeasters and easterlies originated most likely from dry winds that flowed down 114 the slopes of the southern and eastern EIS margins where they picked up and turned gradually into northeasters and easterlies. By blowing over the bare proglacial EIS areas, they generated dust emissions, carried the dust westwards implying dust 116 depositions in areas west of the respective dust sources.

#### 3.2 East Sector Winds and Cyclones over Central Europe

118 In agreement with this hypothesis, glacial simulations for 90 ka ago evidenced katabatic winds over the EIS (Krinner et al., 2004) and GCM simulations for the LGM indicate prevailing east sector winds over central and eastern Europe (COHMAP 120 Members, 1988; Ludwig et al., 2016). In Germany, several aeolian sediment records that are dated to the LGM originated from more eastern sources (Dietrich and Seelos, 2010; Krauß et al., 2016; Römer et al., 2016). In contrast to the dominant present-day 122 anticyclones and west sector winds (southwesters, westerlies and northwesterners), east sector winds (36%) and cyclones (22%) prevailed over central Europe during the LGM (Table 2). These east sector winds are associated with a strong EIS-High (Fig. 2a 124 and COHMAP Members, 1988). This finding is consistent with the analysis of the LGM storm tracks that deviated from their present-day course (Hofer et al., 2012), running either along central Europe, the Mediterranean or the Nordic Seas (Florineth 126 and Schlüchter, 2000; Luetscher et al., 2015; Ludwig et al., 2016). Their Mediterranean course is consistent with the Alpine, western, and southern European climate proxies (Luetscher et al., 2015). In addition, the proxies indicate a storm track branch 128 split-off over the Adriatic that ran past the Eastern Alps to central Europe (Florineth and Schlüchter, 2000; Luetscher et al., 2015; Újvári et al., 2017). These proxy-based findings are in line with the more frequent cyclones in central Europe during the 130 LGM (Table 2). This, in turn, can be related to the stronger and southwards shifted jet stream (Luetscher et al., 2015; Ludwig et al., 2016) and the missing Scandinavian cyclone tracks, which were deflected southwards by the blocking EIS-High. As 132 a result, their frequency increased over central Europe (Table 2), consistent with susceptibility- and grain-size-based results that suggest more frequent storms over western Europe. The east sector winds, which more than doubled in frequency in 134 comparison to today (36% compared to 17%, Table 2) need to be incorporated to establish a more complete understanding of the main drivers of the dust cycle in Europe during the LGM (Fig. 9a). These winds are also evidenced by northern-central 136 European grain-size records for the Late Pleniglacial (Bokhorst et al., 2011). Sediment layers attributed to east wind dated to



138 36–18 ka BP are abundant in the Dehner Maar sediments (Eifel, Germany, 6.5°E, 50.3°N; Dietrich and Seelos, 2010). Their provenance showed that up to every fifth dust storm over the Eifel came from the east (Dietrich and Seelos, 2010).

Our findings are in agreement with fieldwork-based results of Römer et al. (2016), who found evidence for strong east sector  
140 winds over northern, central and western Germany for 23 to 20 ka ago. Also loess in the Harz Foreland indicates a shift to prevailing east sector winds for the LGM (Krauß et al., 2016). The location of aeolian ridges along rivers in northeastern  
142 Belgium and a core transect near Leuven also support our finding by evidencing northeasters for the Late Pleniglacial (Renssen et al., 2007). In addition, northerlies, northeasters and easterlies were inferred from loess deposits west of the Maas (Renssen et al., 2007). Also for Denmark, wind-polished boulders evidence dominant easterlies and southeasters in the period of 22 to  
144 17 ka ago (Renssen et al., 2007). The CWT frequency distribution for the LGM (Table 2) contradicts the finding (Renssen et al., 2007) of prevailing west sector winds during the LGM in central Europe (0–30°E, 40–55°N). The distribution also contrasts with the finding (Sima et al., 2013) of prevailing winds from west-northwest in eastern central Europe, in particular for the area  
148 around Stayky (31°E, 50°N). More precisely, the CWT-W and CWT-NW regimes occurred in eastern central Europe in sum for less than 10% of the times during the LGM (Table 2), which is even less than the expectation value for a single weather  
150 type in case of a uniform CWT frequency distribution. On the contrary, the significant role of the east sector winds (Table 2) is consistent with the deposits on the west bank of the Dnieper (Sima et al., 2013), which are also the loess deposits closest to  
152 Stayky. In addition, sandy soil texture and sand dunes indicate prevailing northerlies and northeasters over Dobrudja (28.18°E, 44.32°N), the eastern Walachian Plain (both located in Romania) and Stary Kaydaky (Ukraine, 35.12°E, 48.37°N; Buggle et al., 2008). The northerlies over Ukraine originated from katabatic winds descending from the EIS (Buggle et al., 2008). The  
154 high aridity and grain size variations of the Surduk and Stari Bezradychy records (Serbia/Ukraine, Supplementary Table S1) evidence prevailing dry and periodically strong east sector winds (Antoine et al., 2009a; Bokhorst et al., 2011).

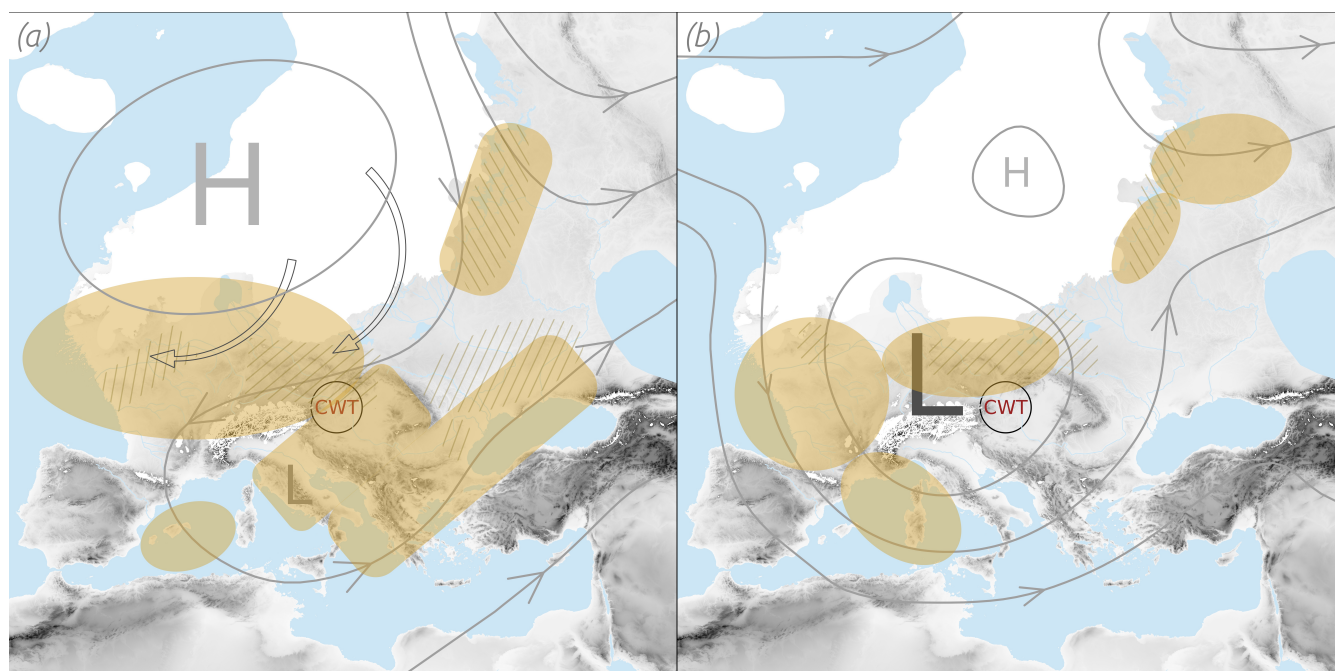


**Figure 2.** Conceptual model explaining the linkage between the European dust cycle during the Last Glacial Maximum and the loess deposits. The main dust deposition areas (filled), emission areas (hatched) and pressure patterns (H/L: high/low pressure) are highlighted. The center of the region for the Circulation Weather Type analysis is denoted with CWT. (a) Northeasters, easterlies and southeasters (the east sector winds; transparent arrows with black perimeter) caused by the semi-permanent high-pressure over the Eurasian ice sheet (white) prevailed 36% of the time over central Europe (Table 2). (b) The cyclonic weather type regimes which prevailed 22% of the time over central Europe (Table 2).

**Table 2.** Circulation Weather Type occurrence frequencies (%) for central Europe (centered at 17.5°E and 47.5°N) during the LGM and the Pre-Industrial period (PI). The frequencies are based on the LGM and the PI simulation of the Max-Planck-Institute Earth System Model. The Circulation Weather Type classes are: Cyclonic (C), Anticyclonic (A), Northeast (NE), East (E) followed by the remaining standard wind directions.

	C	A	NE	E	SE	S	SW	W	NW	N
LGM	22.2	8.9	12.4	13.4	10.2	9.7	6.8	4.3	5.0	7.0
PI	10.6	24.1	7.3	5.2	4.9	7.6	11.6	11.1	9.4	8.3





### 3.3 Dust Emissions from the Eurasian ice sheet margin

158 The model-simulated dust emission (Fig. 3) indicates that most dust in Europe was emitted from the less elevated corridor  
between the Alps, the Black Sea and the EIS (45–55°N). This finding is consistent with loess-based dust-flux estimates (Újvári  
160 et al., 2010). The highest emission rates ( $>10^5$  g m<sup>-2</sup> yr<sup>-1</sup>) occurred along the southern EIS margin (15–18°E, 51–53°N, Fig. 3).  
This location is in line with the location of the highest emissions found in the Greenland stadial GCM simulation of Sima et al.  
162 (2013), yet, our simulation indicates a larger upper limit for the emission rates (1000 g m<sup>-2</sup> yr<sup>-1</sup>). Our results also show high  
emissions in the dry-fallen Channel and the German Bight (Fig. 3). For the latter, they compare well with a glacial climate  
164 simulation that calculated an average emission of 140 and a maximal emission of  $>200$  g m<sup>-2</sup> yr<sup>-1</sup> (Sima et al., 2009).

The loess deposits (Újvári et al., 2010) and the model results are consistent in that the Carpathian Basin was both a dust  
166 source and a dust sink (Fig. 3 and 4). Major dust sources surrounding the Carpathians and the Eastern Alps (Fig. 3) are in  
line with deposits in Serbia and the Carpathian Basin (Újvári et al., 2010; Bokhorst et al., 2011). The dust emissions from  
168 the Lower Danube Basin (Fig. 3) are in agreement with plentiful sediment supply, strong winds and dry conditions inferred  
from the plateau loess in Urluia, located near the Black Sea in southeastern Romania (Fitzsimmons and Hambach, 2014).  
170 Also the emissions from the western Black Sea littoral (Fig. 3) are consistent with provenance analyses of Eastern Dobrogea  
loess in the Lower Danube Basin (Jipa, 2014). Our results indicate a close relationship between strong dust emissions and  
172 low terrains (or basins). This relationship is found for the North Sea Basin and the European plains bordering the EIS, the  
Caucasus, the Carpathians or the Massif Central (Fig. 1 and 3). The dust emissions from the EIS margin and from the foothills  
174 of the European mountains (Fig. 3) are consistent with the loess-based finding of significant aeolian dust contributions from  
glaciogenic and orogenic dust sources (Újvári et al., 2010).

### 176 3.4 Conforming Dust Deposition and Loess Accumulation Rates

The European loess belt (Kukla, 1977; Little et al., 2002; Haase et al., 2007; Sima et al., 2009) is the key to validating paleo  
178 climate-dust simulations for Europe. It corresponds to the unglaciated European area that was bounded northwards by the  
EIS and southwards by the Alps, the Dinaric Alps and the Black Sea. Compared to the GCM-based dust simulations, our  
180 simulated dust deposition rates ( $F_D$ ; Fig. 4) are in better quantitative agreement (by orders of magnitude) with the loess-based  
reconstructed MARs (Supplementary Table S1). For this study, the deposition rate of particles smaller than 12 μm (20 μm)  
182 in diameter is denoted as  $F_{D12}$  ( $F_{D20}$ ).  $F_{D20}$  and  $F_{D12}$  are calculated based on the dynamic ( $F_{D20\text{DD}}$ ,  $F_{D12\text{DD}}$ ) and the  
statistic dynamic ( $F_{D20\text{SD}}$ ,  $F_{D12\text{SD}}$ ) downscaling simulations. The dynamic and statistic dynamic downscaling resulted in  
184 similar  $F_D$  values for central Europe, confirming the suitability of the statistic dynamic downscaling (Fig. 4).

During the LGM, the largest  $F_{D20}$  ( $>10^5$  g m<sup>-2</sup> yr<sup>-1</sup>) occurred in western Poland (Fig. 4a). Slightly lower  $F_{D20}$  ( $10^4$ –  
186  $10^5$  g m<sup>-2</sup> yr<sup>-1</sup>) were found in adjacent areas, e.g. in eastern Germany.  $F_{D20}$  was  $10^3$ – $10^4$  g m<sup>-2</sup> yr<sup>-1</sup> on the North German  
Plain, in the dry-fallen German Bight, eastern England, northern and western France, the Benelux and southeast of the Carpathi-  
188 ans. Regional deposition maxima of  $10^3$ – $10^4$  g m<sup>-2</sup> yr<sup>-1</sup> occurred along the French LGM coastline (46–48°N), on the eastern  
side of the Carpathians (44–47°N, including the eastern Romanian Danube Plain) and near the Caucasus (44–45°N, Fig. 4a).

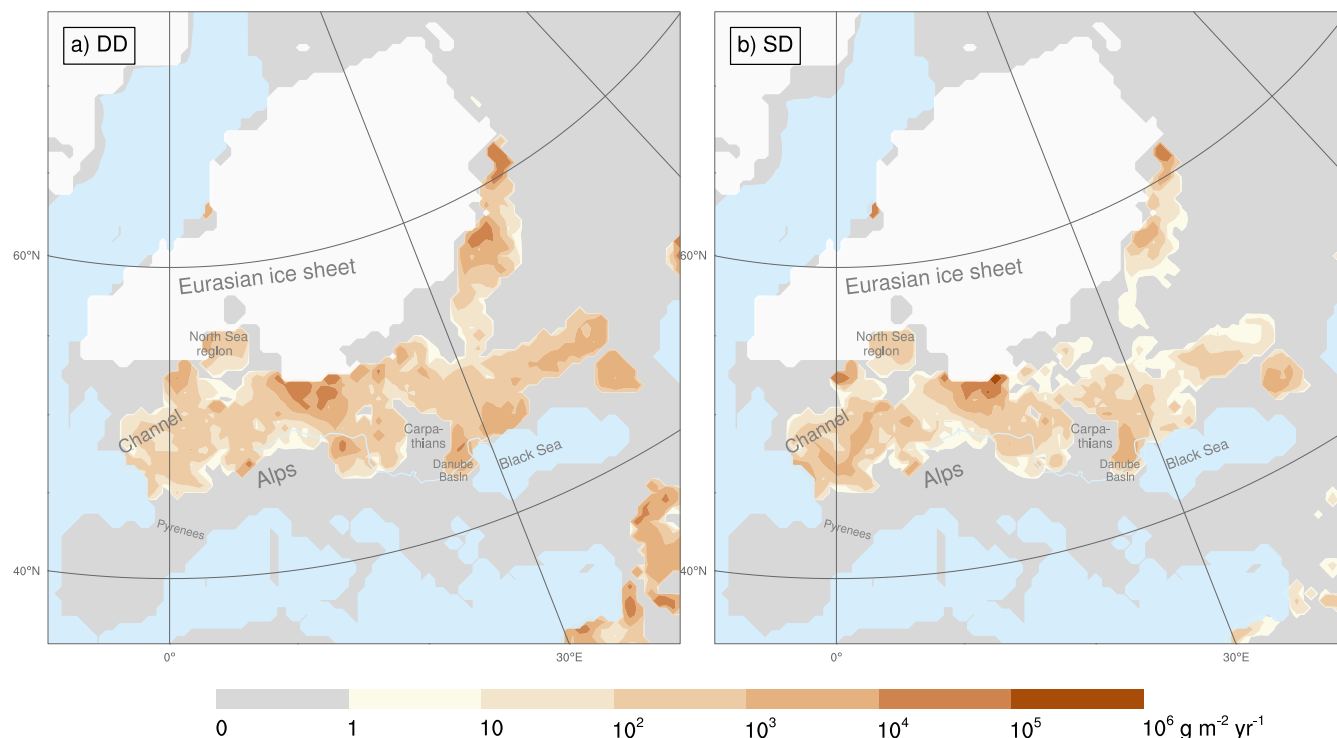


**Figure 3.** Dust emission rates for the Last Glacial Maximum. These reconstructions are based on a) dynamic downscaling (DD) and b) statistic dynamic downscaling (SD). Ice sheet extents (white overlay), Danube (light-blue line).

190 They coincide with today's extensive loess derivatives along the Atlantic coastline of France, at the European foothills north of  
42°N and with the loess thickness maximum in the Romanian Danube Plain (Haase et al., 2007; Jipa, 2014). The quality of  
192 the simulation is recognizable in the Carpathian Basin where the simulated  $F_{D20}$  of 100–1000  $\text{g m}^{-2} \text{yr}^{-1}$  (Fig. 4a) are in good  
agreement with the MARs (200–500  $\text{g m}^{-2} \text{yr}^{-1}$ ) and the fact that half of the Basin is covered by loess and clay of aeolian  
194 origin (Varga et al., 2012). By definition, the MAR is reconstructed from all deposited particles independent of their size. In  
Ukraine and at the eastern margins of the EIS,  $F_{D20}$  of 100–1000  $\text{g m}^{-2} \text{yr}^{-1}$  are in line with the MARs (Fig. 4a). Over Ukraine  
196 and consistent with our results, dust transport and deposition by east sector winds is evidenced by loess deposits on the west  
bank of the Dnieper (Sima et al., 2013).

198 The MARs of a few loess sites are higher than the  $F_{D20}$  in their surrounding. Such an underestimation could be explained  
by particles larger than  $20 \mu\text{m}$  which are not taken into account by the  $F_{D20}$ . For some regions, the MARs of closely related  
200 sites vary over orders of magnitude, e.g. between  $10^2$  and  $10^4 \text{g m}^{-2} \text{yr}^{-1}$  near the Rhine and in Belgium (Fig. 4a). This may  
be due to strong small scale variability, loess dating uncertainties (Singhvi et al., 2001; Renssen et al., 2007) or age model  
202 inaccuracies (Bettis et al., 2003). For western Germany, a transition from higher  $F_{D20}$  ( $10^3$ – $10^4 \text{g m}^{-2} \text{yr}^{-1}$ ) in its northeast  
to lower  $F_{D20}$  ( $10^2$ – $10^3 \text{g m}^{-2} \text{yr}^{-1}$ ) in its southwest was found (Fig. 4a). For a few sites in southwestern Germany, Austria,  
204 Ukraine and along the Danube,  $F_{D20}$  is an order of magnitude lower than the respective MARs (Fig. 4a). Given the 50 km grid

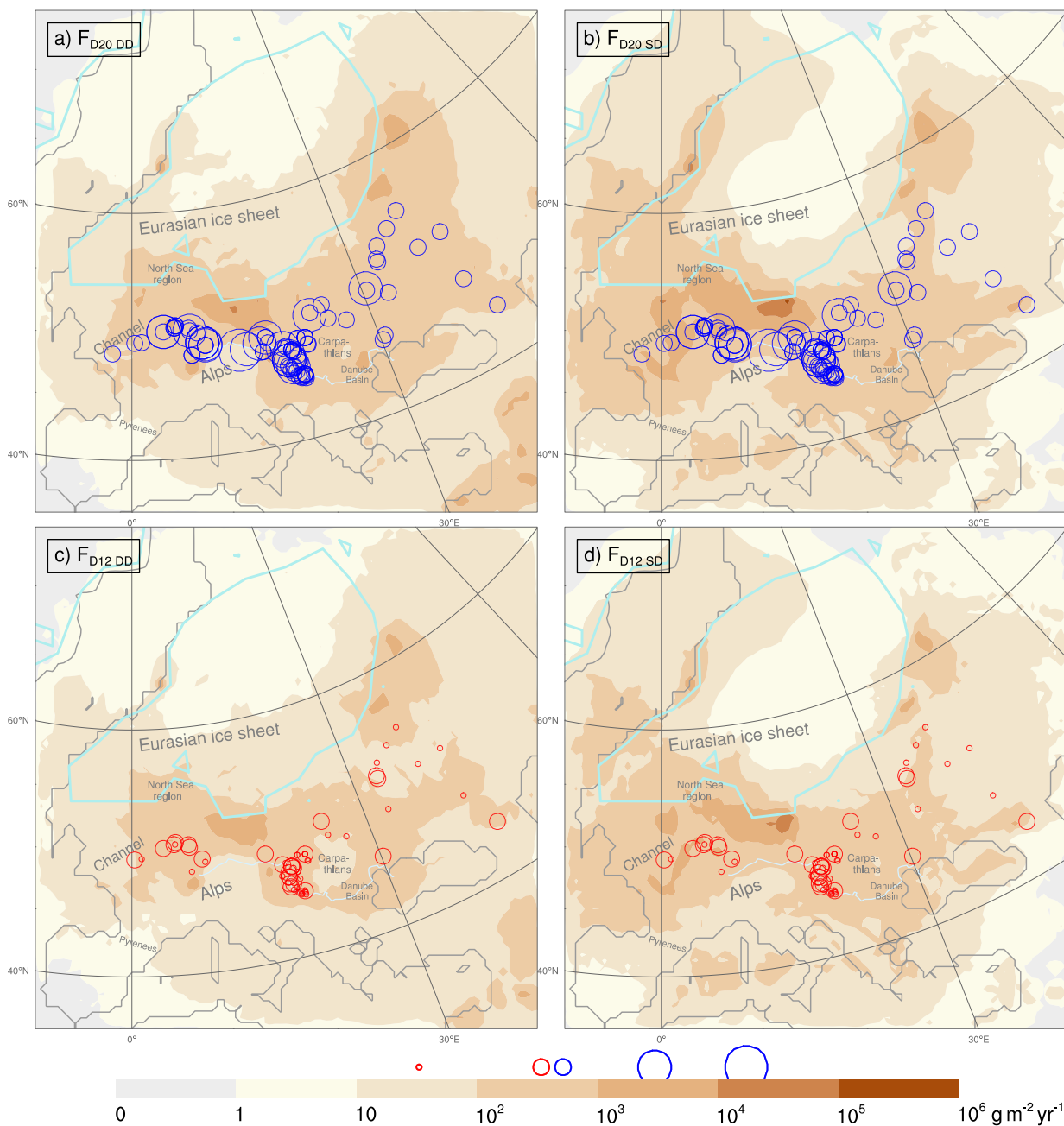


**Figure 4.** Dust deposition rates for the Last Glacial Maximum, comprising particles of up to  $20 \mu\text{m}$  diameter ( $F_{D20}$ ) using (a) dynamic downscaling ( $F_{D20 \text{ DD}}$ ) and (b) statistic dynamic downscaling ( $F_{D20 \text{ SD}}$ ). (c) and (d) as (a) and (b), but for particles up to  $12 \mu\text{m}$  ( $F_{D12}$ ). Each blue circle size represents one mass accumulation rate (MAR) magnitude. Each red circle size represents one reduced mass accumulation rate (MAR10) magnitude. MAR and MAR10 values compiled in Supplementary Table S1. The simulation-based ( $F_{D20}$ ,  $F_{D12}$ ) and the fieldwork-based (MAR, MAR10) rates result from independent data. Delineated are the Danube (light blue), the coastlines (grey; Braconnot et al., 2012) and the ice sheet extents (turquoise; Cline et al., 1984).



spacing of the WRF-Chem-LGM simulation, this may be attributed to missing local dust sources, such as dry-fallen riverbeds  
206 and floodplains. Possibly, the MARs of these sites are also inferred from particles that were predominantly larger than 20  $\mu\text{m}$   
yet data on particle sizes is not available.

### 208 3.5 Seasonal dust cycle patterns

During the LGM, the strongest emission and deposition in Europe occurred in summer, followed by autumn and spring  
210 (Fig. 5 and 6). The areas with the overall highest emission were also those with the highest seasonal emission (Fig. 3 and 5). The  
spring and winter emissions have the same order of magnitude. The low winter and spring emission rates along the EIS margin  
212 were caused by the then extensive snow cover there. During winter, emissions peaked only in northern France, consistent with  
its small snow cover and the vegetation cover that was prescribed to the WRF-Chem-LGM. Major dust emissions occurred  
214 from the Carpathian Basin and along the northwest coast of the Black Sea. During spring, slightly attenuated emissions are  
simulated for France, despite of the decreasing snow cover but in accordance with its increasing vegetation cover. Considerably  
216 higher emission rates are simulated from along the German and Polish EIS margin where the snow cover had retreated. For  
eastern Europe, the growing vegetation cover and the slight soil moisture increase account for partly lower spring than winter  
218 emission rates. The soil moisture increase possibly resulted from meltwater of the retreating snow cover. The highest emission  
rates occurred during summer and were located along the German and Polish EIS margin. Slightly lower emissions are found  
220 to the east of the EIS. These findings are coherent with the surface properties of these areas during summer, i.e. they were  
mostly snow-free and the least moist. During fall, the snow cover increased, causing a decrease of dust emissions, except for  
222 the area north of the Black Sea which encountered its annual maximum. This maximum can be attributed to the retreat of the  
vegetation cover and the dry soil conditions there.

224 The winter CWT distribution indicates prevailing east sector winds (37%) in contrast to cyclonic regimes, which occurred  
much less frequently than on annual average (13%; Table 2 and 3). The winter deposition rates northwest of the Alps were  
226 considerably above, while the rates at the central and eastern European EIS margin were below the annual average (Fig. 4  
and 6a). In western Europe, the highest deposition rates occurred near the sources, yet a considerable dust fraction was also  
228 transported and deposited to the west and northwest of the sources, which requires east sector winds. Low deposition rates were  
found for southern France, however marked depositions occurred when subjected to cyclonic regimes (Fig. 9b). The deposition  
230 pattern for the central Mediterranean area (Italy, the Adriatic) suggests significant dust transport by east sector winds and  
anticyclonic winds, in sum prevailing 51% of the times. In eastern Europe, considerable winter depositions rates covered areas  
232 south of the dust sources, in particular the western Black Sea and regions south of the Danube. This indicates a significant  
contribution to the dust transport by northerlies (6%), northeasters (12%) and the anticyclonic regimes (14%).

234 Also the spring deposition rates evidence the importance of the east sector winds (42%, Table 3) for the dust cycle. In  
western Europe, major deposition areas are to the west and northwest of the sources, while they are to the west and southwest  
236 in eastern Europe (Fig. 6b). An increase of the dust transport towards the south in western, and towards the north in eastern  
Europe indicates an increasing role of the cyclonic regimes (27%) during the spring.



238 The summer deposition rates are distributed zonally along the EIS margin, suggesting an approximately latitude-parallel dust  
transport by west (21%) and/or east sector (24%) wind directions. In addition, the northern flanks of cyclonic regimes (24%)  
240 likely contributed to a westwards dust transport. Over north-easternmost Europe (40E, 62N), the deposition rates suggest east  
sector winds. The autumn deposition rates over western and central Europe show a westward running plume from the southern  
242 EIS margin over Germany and Poland, corroborating the major role of the east sector winds (38%) for the dust cycle. The high  
deposition rates in eastern Europe suggest that also the cyclonic regimes (19%) contributed during fall.

**Table 3.** Seasonal CWT occurrence frequencies (%) for central Europe (centered at 17.5°E and 47.5°N) during the LGM. The frequencies are based on MPI-LGM simulation. The CWT classes are: Cyclonic (C), Anticyclonic (A), Northeast (NE), East (E) followed by the remaining standard wind directions. Sum E is the sum of the east sector winds (NE, E, SE). The seasons are labeled DJF (winter), MAM (spring), JJA (summer) and SON (fall).

	C	A	Sum E	NE	E	SE	S	SW	W	NW	N
DJF	12.6	13.9	37.4	11.8	14.4	11.2	12.9	8.5	5.1	4.1	5.6
MAM	27.1	6.1	41.9	12.9	16.4	12.6	9.7	4.8	2.8	3.6	4.2
JJA	26.8	7.5	24.4	12.8	6.3	5.3	9.3	7.3	6.1	7.9	10.7
SON	18.6	10.0	37.8	12.8	13.6	11.4	10.8	6.8	3.8	5.1	7.0

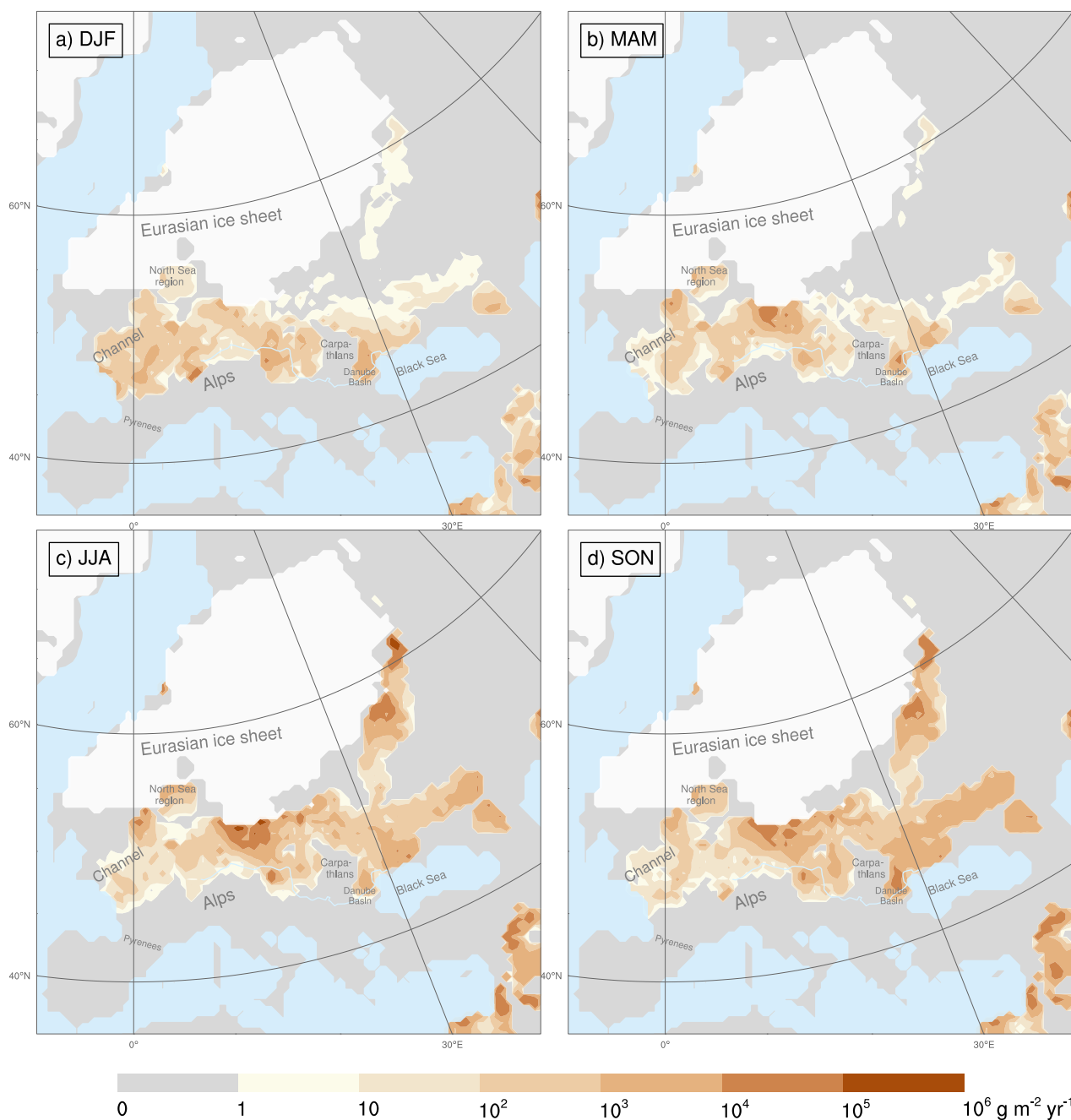


**Figure 5.** Dust emission rates for a) winter (DJF), b) spring (MAM), c) summer (JJA), and d) fall (SON) during the Last Glacial Maximum. This reconstruction is based on dynamic downscaling. The Danube (light-blue line) and the extent of the continental ice sheets (white) are shown.

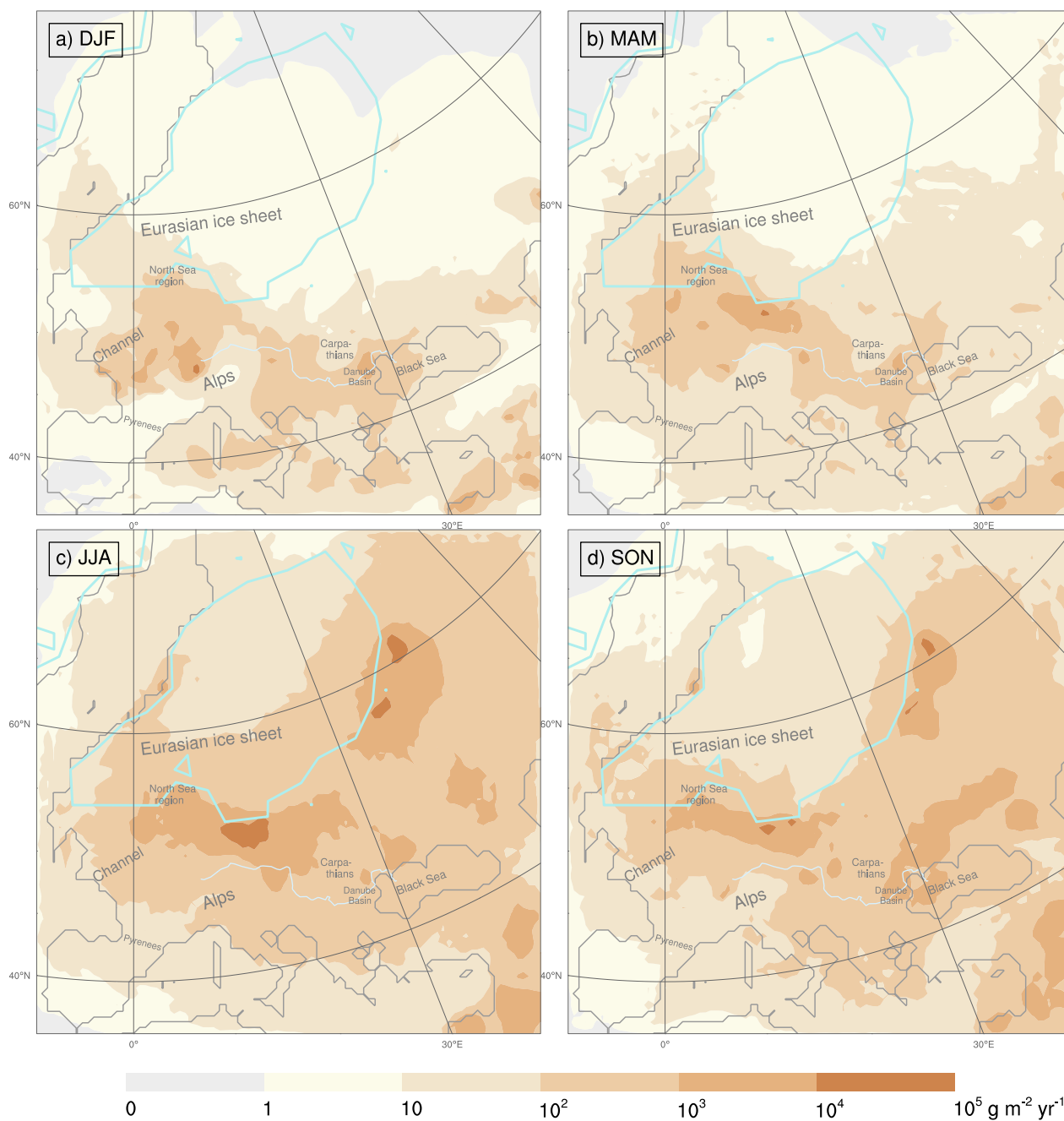


**Figure 6.** Dust deposition rates for a) winter (DJF), b) spring (MAM), c) summer (JJA) and d) autumn (SON) during the Last Glacial Maximum. This reconstruction is based on dynamic downscaling. Ice sheet extents (turquoise; Cline et al., 1984), Danube (light-blue line) and coastlines (grey; Braconnot et al., 2012) are delineated.

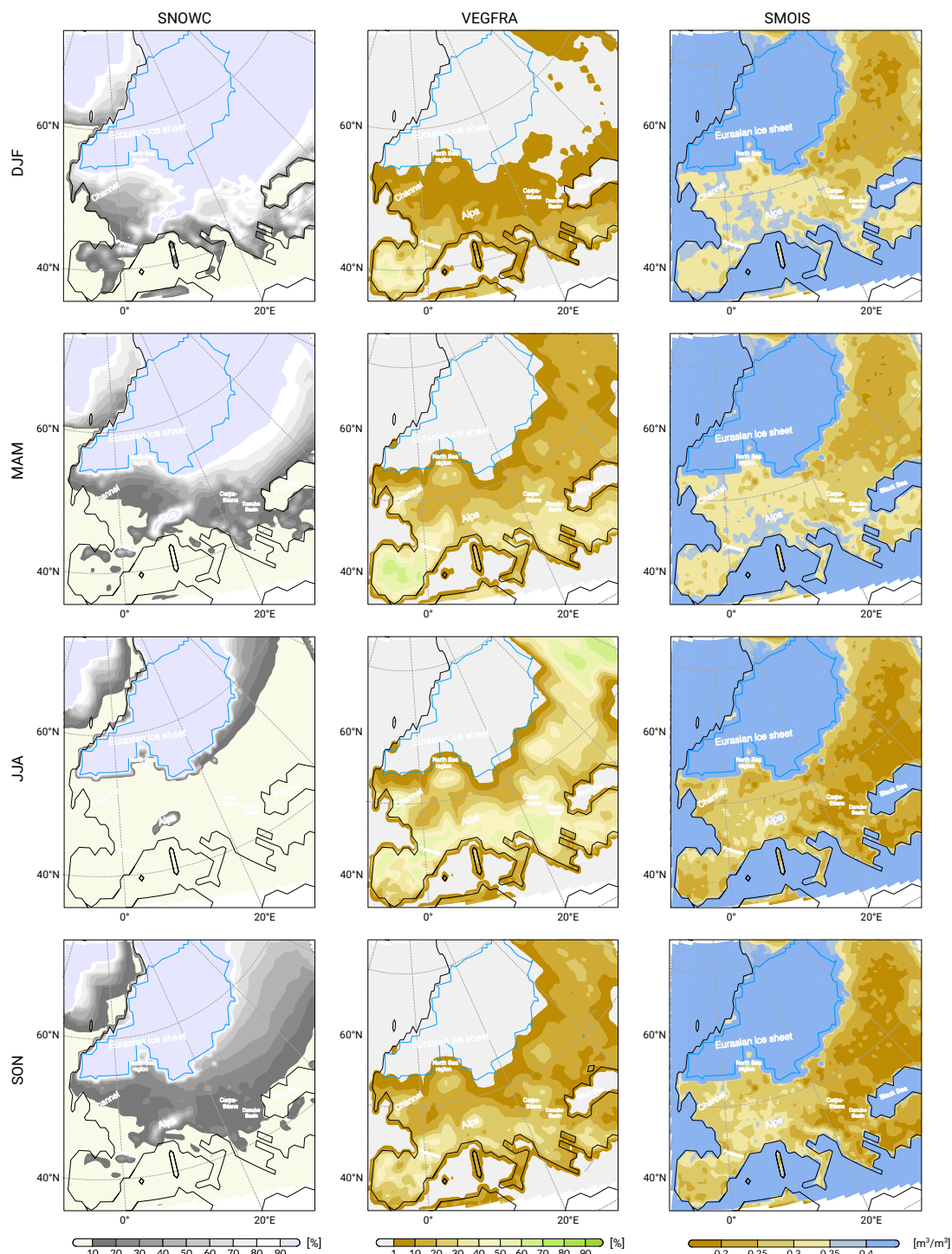


**Figure 7.** Snow cover (%), vegetation cover (%) and soil moisture ( $\text{m}^3/\text{m}^3$ ), resolved for winter (DJF), spring (MAM), summer (JJA) and fall (SON) for the Last Glacial Maximum. These reconstructions are based on dynamic downscaling.





### 244 3.6 Wind regime-based dust cycle decomposition

The wind regime occurrence frequency distribution (Table 2) demonstrates the temporal dominance of the east sector winds during the LGM. This temporal dominance likely shaped the dust cycle but the contribution of each wind regime type has so far not been analyzed. This analysis is provided here by discussing the dust emission and deposition characteristics associated with different CWTs which reveal that the east sector winds caused by far the largest dust emission and depositions during the LGM (Fig. 8a and 9a). In sum, they generated an average emission of  $1111 \text{ g m}^{-2} \text{ yr}^{-1}$  (Fig. 8a) which is more than twice of the rate generated by cyclonic regimes ( $494 \text{ g m}^{-2} \text{ yr}^{-1}$ , Fig. 8b). The west sector winds contributed on average even less to the dust cycle  $375 \text{ g m}^{-2} \text{ yr}^{-1}$  (Fig. 8c). Compared to the southerlies ( $232 \text{ g m}^{-2} \text{ yr}^{-1}$ , Fig. 8d), this rate is low for a wind sector that sums the contribution of three wind directions (SW, W, NW).

The cyclonic wind regimes caused the most heterogeneously distributed emissions (Fig. 8b) with four main centers: the largest located in the German-Polish-Czech border region, another in eastern England and the remaining two near the EIS margin in western Russia. This distribution resembles to a subset of the emission distribution of the east sector winds (Fig. 8a). Together with the location of the CWT reference regions, this resemblance could be explained by the fact that all records classified as cyclonic must center their cyclonic pressure distribution approximately around the central point for the CWT classification ( $17.5^\circ\text{E}$ ,  $47.5^\circ\text{N}$ ). This implies that the corresponding emissions could have been triggered by easterlies on the northern flanks of the cyclones. Dust was hardly emitted from areas on the southern flanks of the cyclones which are commonly affected by fronts and precipitation (Booth et al., 2018). In addition to the dust emission areas that occurred equally during both regimes (cyclonic and east sector winds), the east sector winds also generated emissions in Austria, Slovakia, Hungary, Ukraine, central Germany, the Danube Basin and the North Sea Basin. In contrast, the west sector winds produced a more homogeneous distribution of markedly smaller emission rates extending from western Ukraine to the French Atlantic coast. While northwesterers with a strong northerly component most likely forced emissions from the German-Polish EIS margin, the west sector winds and the southerlies controlled the emissions from France, southwestern Germany, the Channel, and the Alps foreland (Fig. 8c and d). The combination of the emission and deposition rate patterns of the east sector winds (Fig. 8a and 9a) indicates major westwards dust transport along the southern and eastern EIS margin. The conic shape of the deposition rate distribution in western and central Europe (between  $10^2$  and  $10^3 \text{ kg m}^{-2} \text{ yr}^{-1}$ ) suggests that these depositions can be attributed to emissions from more eastern sources. The east sector winds also deposited considerable amounts of dust in and south of the Danube Basin as well as along the Danube.

The deposition rates of the cyclonic regimes (Fig. 9b) indicate two main dust transport directions: westwards over central and eastern Europe, whereas southwards over western Europe. More precisely, dust was transported westwards from Poland to eastern and central Germany, while it was carried southwards from eastern England to the Channel and north-western France up to the Pyrenees foreland. The emission and deposition distributions associated with the west sector winds are almost congruent (Fig. 8c and 9c). Combining them does not reveal a unique dust transport direction by west sector winds, it rather suggests omnidirectional transports; even a westward transport cannot be excluded e.g. to Scotland, Ireland or areas at the Russian EIS margin (Fig. 9c). The depositions caused by southerlies show a north-westward transport over central Europe (Fig. 9d).



278 Considerable amounts of dust (between  $10^3$  and  $10^5$   $\text{kg m}^{-2} \text{yr}^{-1}$ ) were transported from sources in western Poland, eastern  
Germany and Czechia to northern Germany, Denmark, southern Sweden and the North Sea Basin. The deposition pattern also  
280 suggests a north-westward transport in France.



**Figure 8.** Dust emission rate fractions caused by the a) northeasters, easterlies and southeasters, b) cyclonic regimes, c) southwester, westerlies and northwester, and d) southerlies during the Last Glacial Maximum. The simulated emission rates are weighted according to the occurrence frequency of the associated wind regime(s) in the Max-Planck-Institute Earth System Model (Table 2). Dust particles up to  $20 \mu\text{m}$  diameter have been considered. The Danube (light-blue line) and the extent of the continental ice sheets (white) are shown.

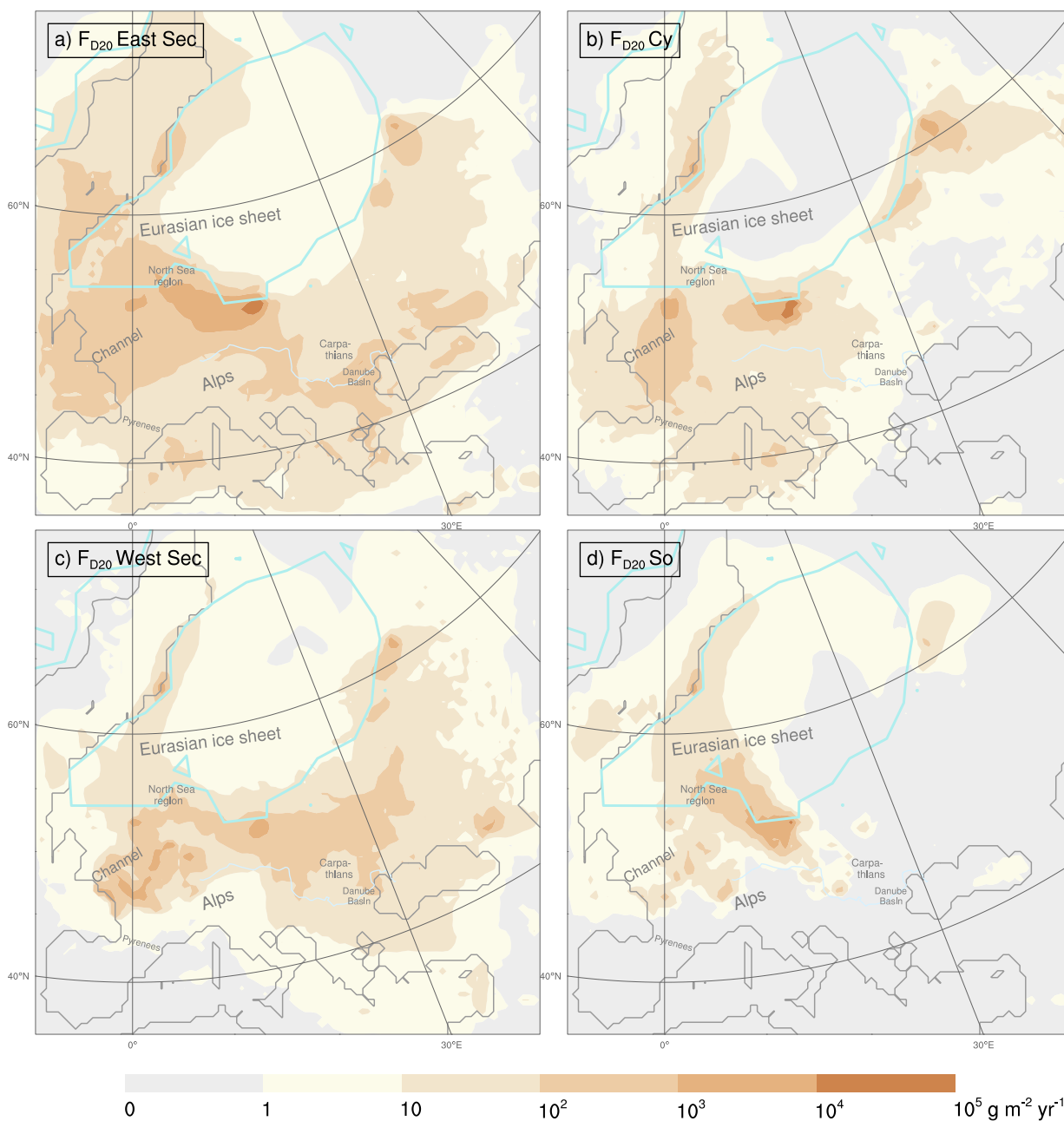


**Figure 9.** Dust deposition rate fractions caused solely by the a) northeasters, easterlies and southeasters, b) cyclonic regimes, c) southwester, westerlies and northwester, and d) the southerlies during the Last Glacial Maximum. The simulated deposition rates are weighted according to the occurrence frequency of the associated wind regime(s) in the Max-Planck-Institute Earth System Model (Table 2). Dust particles up to  $20 \mu\text{m}$  diameter have been considered. The ice sheet extents (turquoise; Cline et al., 1984), the Danube (light blue) and the coastlines (grey; Braconnot et al., 2012) are delineated.



#### 4 Conclusions

282 Compared to previous climate-dust model simulations for the LGM, this study presents a dust cycle reconstruction with dust  
deposition rates that are in much better agreement with the MARs reconstructed from more than 70 different loess deposits  
284 across Europe. By taking into account the effect of different wind directions, a more complete understanding of the dust cycle  
is established. The obtained results corroborate the hypothesis on the linkage between the prevailing dry east sector winds as a  
286 major driver of the LGM dust cycle in central and eastern Europe and the loess deposits.

The study demonstrates that the WRF-Chem-LGM model is capable of simulating the glacial dust cycle including emission,  
288 transport and deposition. In addition, the suitability of the statistic dynamic approach for regional climate-dust simulations is  
proven by the similarity of the dynamic and statistic-dynamic downscaling results. In contrast to the dominant present-day  
290 westerlies over Europe, the CWT analysis revealed dominant east sector (36%) and cyclonic (22%) wind regimes during the  
LGM over central Europe. These east sector winds dominated the LGM dust cycle by far during all but the summer season.  
292 In summer, they were about as frequent as the cyclonic regimes. The dominance of the east sector winds during the LGM is  
corroborated by numerous local proxies for the wind and dust transport directions in Europe.

294 The WRF-Chem-LGM simulations show that almost all dust emission occurred in a corridor that was bounded to the north  
by the EIS and to the south by the Alps and the Black Sea. Within this corridor, the highest emissions were generated from the  
296 dry-fallen flats, the lowlands bordering mountain slopes, and the proglacial areas of the EIS. Most dust was emitted during the  
summers and autumns of the LGM, probably due to the then vanishing snow cover. The largest depositions during the LGM  
298 occurred near the southernmost margin of the EIS (12–19°E;  $10^5 \text{ g m}^{-2} \text{ yr}^{-1}$ ), on the North German Plain including adjacent  
regions and in the southern North Sea region. The agreement between the performed climate-dust simulations for the LGM  
300 and the reconstructed MARs from loess deposits corroborates the proposed LGM dust cycle hypothesis.

*Author contributions.* EJS, PL and YS designed the concept of the study. PL performed the dynamic downscaling simulation and created  
302 Figure 7. EJS performed the statistic dynamic downscaling, compared the results with the proxy data including the reconstructed loess mass  
accumulation rates, created the tables and the remaining figures. EJS wrote the paper with contributions from PL and YS.

304 *Competing interests.* The authors declare that they have no conflict of interest.

*Acknowledgements.* This research was funded by the Deutsche Forschungsgemeinschaft (DFG) through the Collaborative Research Center  
306 806 “Our Way to Europe” (CRC806). P. Ludwig thanks the Helmholtz initiative REKLIM for funding. We thank the German Climate  
Computing Centre (DKRZ, Hamburg) for providing the MPI-ESM data and computing resources (project 965). We thank the Regional  
308 Computing Center (University of Cologne) for providing support and computing time on the high performance computing system CHEOPS.



We thank Qian Xia for preparing model boundary condition data. We thank F. Lehmkuhl, the CRC806 (second phase) members of his group  
310 and J. G. Pinto for helpful discussions and comments.



## References

- 312 Albani, S., Mahowald, N. M., Murphy, L. N., Raiswell, R., Moore, J. K., Anderson, R. F., McGee, D., Bradtmiller, L. I., Delmonte, B.,  
Hesse, P. P., and Mayewski, P. A.: Paleodust variability since the Last Glacial Maximum and implications for iron inputs to the ocean,  
314 *Geophysical Research Letters*, 43, 3944–3954, <https://doi.org/10.1002/2016GL067911>, 2016.
- Antoine, P., Rousseau, D.-D., Fuchs, M., Hatté, C., Gauthier, C., Marković, S. B., Jovanović, M., Gaudenyi, T., Moine, O., and Rossignol, J.:  
316 High-resolution record of the last climatic cycle in the southern Carpathian Basin (Surduk, Vojvodina, Serbia), *Quaternary International*,  
198, 19–36, <http://dx.doi.org/10.1016/j.quaint.2008.12.008>, 2009a.
- 318 Antoine, P., Rousseau, D.-D., Moine, O., Kunesch, S., Hatté, C., Lang, A., Tissoux, H., and Zöller, L.: Rapid and cyclic aeolian deposition  
during the Last Glacial in European loess: a high-resolution record from Nussloch, Germany, *Quaternary Science Reviews*, 28, 2955–2973,  
320 <http://dx.doi.org/10.1016/j.quascirev.2009.08.001>, 2009b.
- Austermann, J., Mitrovica, J. X., Latychev, K., and Milne, G. A.: Barbados-based estimate of ice volume at Last Glacial Maximum affected  
322 by subducted plate, *Nature Geoscience*, 6, 553–557, <https://doi.org/10.1038/ngeo1859>, 2013.
- Bartlein, P. J., Harrison, S. P., Brewer, S., Connor, S., Davis, B. A. S., Gajewski, K., Guiot, J., Harrison-Prentice, T. I., Henderson, A.,  
324 Peyron, O., and et al.: Pollen-based continental climate reconstructions at 6 and 21 ka: a global synthesis, *Climate Dynamics*, 37, 775–802,  
<http://dx.doi.org/10.1007/s00382-010-0904-1>, 2011.
- 326 Bettis, E. A., Muhs, D. R., Roberts, H. M., and Wintle, A. G.: Last Glacial loess in the conterminous USA, *Quaternary Science Reviews*, 22,  
1907–1946, [http://dx.doi.org/10.1016/S0277-3791\(03\)00169-0](http://dx.doi.org/10.1016/S0277-3791(03)00169-0), 2003.
- 328 Bokhorst, M., Vandenberghe, J., Sümegei, P., Łanczont, M., Gerasimenko, N., Matviishina, Z., Marković, S., and Frechen, M.: Atmospheric  
circulation patterns in central and eastern Europe during the Weichselian Pleniglacial inferred from loess grain-size records, *Quaternary*  
330 *International*, 234, 62–74, <http://dx.doi.org/10.1016/j.quaint.2010.07.018>, 2011.
- Booth, J. F., Naud, C. M., and Willison, J.: Evaluation of Extratropical Cyclone Precipitation in the North Atlantic Basin: An Analysis of  
332 ERA-Interim, WRF, and Two CMIP5 Models, *J. of Climate*, 31, 2345–2360, <https://doi.org/10.1175/JCLI-D-17-0308.1>, <https://doi.org/10.1175/JCLI-D-17-0308.1>, 2018.
- 334 Braconnot, P., Harrison, S. P., Kageyama, M., Bartlein, P. J., Masson-Delmotte, V., Abe-Ouchi, A., Otto-Bliesner, B., and Zhao, Y.: Evaluation  
of climate models using palaeoclimatic data, *Nature Climate Change*, 2, 417–424, <http://dx.doi.org/10.1038/nclimate1456>, 2012.
- 336 Buggle, B., Glaser, B., Zöller, L., Hambach, U., Marković, S., Glaser, I., and Gerasimenko, N.: Geochemical characterization and origin of  
Southeastern and Eastern European loesses (Serbia, Romania, Ukraine), *Quaternary Science Reviews*, 27, 1058–1075, <http://dx.doi.org/10.1016/j.quascirev.2008.01.018>, 2008.
- 338 Chin, M., Rood, R. B., Lin, S.-J., Müller, J.-F., and Thompson, A. M.: Atmospheric sulfur cycle simulated in the global model GO-  
340 CART: Model description and global properties, *J. of Geophysical Research: Atmospheres*, 105, 24 671–24 687, <http://dx.doi.org/10.1029/2000JD900384>, 2000.
- 342 Clark, P. U. and Mix, A. C.: Ice sheets and sea level of the Last Glacial Maximum, *Quaternary Science Reviews*, 21, 1–7,  
[https://doi.org/10.1016/S0277-3791\(01\)00118-4](https://doi.org/10.1016/S0277-3791(01)00118-4), 2002.
- 344 Clark, P. U., Dyke, A. S., Shakun, J. D., Carlson, A. E., Clark, J., Wohlfarth, B., Mitrovica, J. X., Hostetler, S. W., and McCabe, A. M.:  
The Last Glacial Maximum, *Science*, 325, 710–714, <https://doi.org/10.1126/science.1172873>, <http://dx.doi.org/10.1126/science.1172873>,  
346 2009.



- Cline, R. M. L., Hays, J. D., Prell, W. L., Ruddiman, W. F., Moore, T. C., Kipp, N. G., Molfino, B. E., Denton, G. H., Hughes, T. J., and  
348 Balsam, W. L.: The Last Interglacial Ocean, *Quaternary Research*, 21, 123–224, [https://doi.org/10.1016/0033-5894\(84\)90098-X](https://doi.org/10.1016/0033-5894(84)90098-X), 1984.
- COHMAP Members: Climatic Changes of the Last 18,000 Years: Observations and Model Simulations, *Science*, 241, 1043–1052,  
350 <https://doi.org/10.1126/science.241.4869.1043>, 1988.
- Dietrich, S. and Seelos, K.: The reconstruction of easterly wind directions for the Eifel region (Central Europe) during the period 40.3 to  
352 12.9 ka BP, *Climate of the Past*, 6, 145–154, <http://dx.doi.org/10.5194/cp-6-145-2010>, 2010.
- Fast, J. D., Gustafson, W. I., Easter, R. C., Zaveri, R. A., Barnard, J. C., Chapman, E. G., Grell, G. A., and Peckham, S. E.: Evolution of  
354 ozone, particulates, and aerosol direct radiative forcing in the vicinity of Houston using a fully coupled meteorology-chemistry-aerosol  
model, *J. of Geophysical Research: Atmospheres*, 111, n/a–n/a, <http://dx.doi.org/10.1029/2005JD006721>, d21305, 2006.
- 356 Fitzsimmons, K. E. and Hambach, U.: Loess accumulation during the last glacial maximum: Evidence from Urluia, southeastern Romania,  
*Quaternary International*, 334–335, 74–85, <https://doi.org/10.1016/j.quaint.2013.08.005>, <http://dx.doi.org/10.1016/j.quaint.2013.08.005>,  
358 2014.
- Fitzsimmons, K. E., Marković, S. B., and Hambach, U.: Pleistocene environmental dynamics recorded in the loess of the middle and lower  
360 Danube basin, *Quaternary Science Reviews*, 41, 104–118, <http://dx.doi.org/10.1016/j.quascirev.2012.03.002>, 2012.
- Florineth, D. and Schlüchter, C.: Alpine Evidence for Atmospheric Circulation Patterns in Europe during the Last Glacial Maximum, *Qua-*  
362 *ternary Research*, 54, 295–308, <http://dx.doi.org/10.1006/qres.2000.2169>, 2000.
- Gasse, F., Vidal, L., Develle, A.-L., and Van Campo, E.: Hydrological variability in the Northern Levant: a 250 ka multiproxy record from  
364 the Yammoūneh (Lebanon) sedimentary sequence, *Climate of the Past*, 7, 1261–1284, <http://dx.doi.org/10.5194/cp-7-1261-2011>, 2011.
- Ginoux, P., Chin, M., Tegen, I., Prospero, J. M., Holben, B., Dubovik, O., and Lin, S.-J.: Sources and distributions of dust aerosols simulated  
366 with the GOCART model, *J. of Geophysical Research: Atmospheres*, 106, 20 255–20 273, <http://dx.doi.org/10.1029/2000JD000053>, 2001.
- Giorgetta, M. A., Jungclaus, J., Reick, C. H., Legutke, S., Bader, J., Böttinger, M., Brovkin, V., Crueger, T., Esch, M., Fieg, K., and et al.:  
368 Climate and carbon cycle changes from 1850 to 2100 in MPI-ESM simulations for the Coupled Model Intercomparison Project phase 5,  
*J. of Advances in Modeling Earth Systems*, 5, 572–597, <http://dx.doi.org/10.1002/jame.20038>, 2013.
- 370 Grell, G. A., Peckham, S. E., Schmitz, R., McKeen, S. A., Frost, G., Skamarock, W. C., and Eder, B.: Fully coupled “online” chemistry  
within the WRF model, *Atmospheric Environment*, 39, 6957–6975, <http://dx.doi.org/10.1016/j.atmosenv.2005.04.027>, 2005.
- 372 Haase, D., Fink, J., Haase, G., Ruske, R., Pécsi, M., Richter, H., Altermann, M., and Jäger, K.-D.: Loess in Europe—its spatial distribution  
based on a European Loess Map, scale 1:2,500,000, *Quaternary Science Reviews*, 26, 1301–1312, <http://dx.doi.org/10.1016/j.quascirev.2007.02.003>, 2007.  
374
- Heyman, B. M., Heyman, J., Fickert, T., and Harbor, J. M.: Paleo-climate of the central European uplands during the last glacial maximum  
376 based on glacier mass-balance modeling, *Quaternary Research*, 79, 49–54, <http://dx.doi.org/10.1016/j.yqres.2012.09.005>, 2013.
- Hofer, D., Raible, C. C., Dehnert, A., and Kuhlemann, J.: The impact of different glacial boundary conditions on atmospheric dynamics and  
378 precipitation in the North Atlantic region, *Climate of the Past*, 8, 935–949, <http://dx.doi.org/10.5194/cp-8-935-2012>, 2012.
- Hopcroft, P. O., Valdes, P. J., Woodward, S., and Joshi, M. M.: Last glacial maximum radiative forcing from mineral dust aerosols in an Earth  
380 system model, *J. of Geophysical Research: Atmospheres*, 120, 8186–8205, <https://doi.org/10.1002/2015JD023742>, 2015.
- Hughes, A. L. C., Gyllencreutz, R., Lohne, O. S., Mangerud, J., and Svendsen, J. I.: The last Eurasian ice sheets - a chronological database  
382 and time-slice reconstruction, *DATED-1, Boreas*, 45, 1–45, <http://dx.doi.org/10.1111/bor.12142>, 2015.
- Jipa, D. C.: The conceptual sedimentary model of the Lower Danube loess basin: Sedimentogenetic implications, *Quaternary International*,  
384 351, 14–24, <http://dx.doi.org/10.1016/j.quaint.2013.06.008>, 2014.





- Jones, P. D., Hulme, M., and Briffa, K. R.: A comparison of Lamb circulation types with an objective classification scheme, *International J. of Climatology*, 13, 655–663, <https://doi.org/10.1002/joc.3370130606>, <http://dx.doi.org/10.1002/joc.3370130606>, 1993.
- Jones, P. D., Harpham, C., and Briffa, K. R.: Lamb weather types derived from reanalysis products, *International J. of Climatology*, 33, 1129–1139, <https://doi.org/10.1002/joc.3498>, <http://dx.doi.org/10.1002/joc.3498>, 2013.
- Jung, E., Shao, Y., and Sakai, T.: A study on the effects of convective transport on regional-scale Asian dust storms in 2002, *J. of Geophysical Research: Atmospheres*, 110, <http://dx.doi.org/10.1029/2005JD005808>, d20201, 2005.
- Jungclaus, J., Giorgetta, M., Reick, C., Legutke, S., Brovkin, V., Crueger, T., Esch, M., Fieg, K., Fischer, N., Glushak, K., Gayler, V., Haak, H., Hollweg, H.-D., Kinne, S., Kornblueh, L., Matei, D., Mauritsen, T., Mikolajewicz, U., Müller, W., Notz, D., Pohlmann, T., Raddatz, T., Rast, S., Roeckner, E., Salzmann, M., Schmidt, H., Schnur, R., Segschneider, J., Six, K., Stockhause, M., Wegner, J., Widmann, H., Wieners, K.-H., Claussen, M., Marotzke, J., and Stevens, B.: CMIP5 simulations of the Max Planck Institute for Meteorology (MPI-M) based on the MPI-ESM-P model: The Igm experiment, served by ESGF, WDCC at DKRZ, <https://doi.org/10.1594/WDCC/CMIP5.MXEPIg>, 2012.
- Jungclaus, J. H., Fischer, N., Haak, H., Lohmann, K., Marotzke, J., Matei, D., Mikolajewicz, U., Notz, D., and von Storch, J. S.: Characteristics of the ocean simulations in the Max Planck Institute Ocean Model (MPIOM) the ocean component of the MPI-Earth system model, *J. of Advances in Modeling Earth Systems*, 5, 422–446, <http://dx.doi.org/10.1002/jame.20023>, 2013.
- Kang, J.-Y., Yoon, S.-C., Shao, Y., and Kim, S.-W.: Comparison of vertical dust flux by implementing three dust emission schemes in WRF/Chem, *J. of Geophysical Research: Atmospheres*, 116, D09202, <https://doi.org/10.1029/2010JD014649>, 2011.
- Kaplan, J. O., Bigelow, N. H., Prentice, I. C., Harrison, S. P., Bartlein, P. J., Christensen, T. R., Cramer, W., Matveyeva, N. V., McGuire, A. D., Murray, D. F., Razzhivin, V. Y., Smith, B., Walker, D. A., Anderson, P. M., Andreev, A. A., Brubaker, L. B., Edwards, M. E., and Lozhkin, A. V.: Climate change and Arctic ecosystems: 2. Modeling, paleodata-model comparisons, and future projections, *J. of Geophysical Research: Atmospheres*, 108, <http://dx.doi.org/10.1029/2002JD002559>, 2003.
- Koven, C. D. and Fung, I.: Identifying global dust source areas using high-resolution land surface form, *J. of Geophysical Research*, 113, <http://dx.doi.org/10.1029/2008JD010195>, 2008.
- Krauß, L., Zens, J., Zeeden, C., Schulte, P., Eckmeier, E., and Lehmkuhl, F.: A Multi-Proxy Analysis of two Loess-Paleosol Sequences in the Northern Harz Foreland, Germany, *Palaeogeography, Palaeoclimatology, Palaeoecology*, 461, 401–417, <http://dx.doi.org/10.1016/j.palaeo.2016.09.001>, 2016.
- Krinner, G., Mangerud, J., Jakobsson, M., Crucifix, M., Ritz, C., and Svendsen, J. I.: Enhanced ice sheet growth in Eurasia owing to adjacent ice-dammed lakes, *Nature*, 427, 429–432, <http://dx.doi.org/10.1038/nature02233>, 2004.
- Kukla, G.: Pleistocene land—sea correlations I. Europe, *Earth-Science Reviews*, 13, 307–374, [http://dx.doi.org/10.1016/0012-8252\(77\)90125-8](http://dx.doi.org/10.1016/0012-8252(77)90125-8), 1977.
- Kumar, R., Barth, M. C., Pfister, G. G., Naja, M., and Brasseur, G. P.: WRF-Chem simulations of a typical pre-monsoon dust storm in northern India: influences on aerosol optical properties and radiation budget, *Atmospheric Chemistry & Physics*, 14, 2431–2446, <https://doi.org/10.5194/acp-14-2431-2014>, 2014.
- Lambeck, K., Rouby, H., Purcell, A., Sun, Y., and Sambridge, M.: Sea level and global ice volumes from the Last Glacial Maximum to the Holocene, *Proceedings of the National Academy of Science*, 111, 15 296–15 303, <https://doi.org/10.1073/pnas.1411762111>, 2014.
- Lañé, A., Kageyama, M., Salas-Méllia, D., Voltaire, A., Rivière, G., Ramstein, G., Planton, S., Tyteca, S., and Peterschmitt, J. Y.: Northern hemisphere storm tracks during the last glacial maximum in the PMIP2 ocean-atmosphere coupled models: energetic study, seasonal cycle, precipitation, *Climate Dynamics*, 32, 593–614, <http://dx.doi.org/10.1007/s00382-008-0391-9>, 2009.



- 424 Little, E. C., Lian, O. B., Velichko, A., Morozova, T., Nechaev, V., Dlussky, K., and Rutter, N.: Quaternary stratigraphy and optical dating of  
loess from the east European Plain (Russia), *Quaternary Science Reviews*, 21, 1745–1762, [https://doi.org/10.1016/s0277-3791\(01\)00151-2](https://doi.org/10.1016/s0277-3791(01)00151-2), 2002.
- 426 Ludwig, P., Schaffernicht, E. J., Shao, Y., and Pinto, J. G.: Regional atmospheric circulation over Europe during the Last Glacial Maximum  
and its links to precipitation, *J. of Geophysical Research: Atmospheres*, 121, 2130–2145, <http://dx.doi.org/10.1002/2015JD024444>, 2016.
- 428 Ludwig, P., Pinto, J. G., Raible, C. C., and Shao, Y.: Impacts of Surface Boundary Conditions on Regional Climate Model Simulations of  
European Climate during the Last Glacial Maximum, *Geophysical Research Letters*, <http://dx.doi.org/10.1002/2017GL073622>, 2017.
- 430 Luetscher, M., Boch, R., Sodemann, H., Spötl, C., Cheng, H., Edwards, R. L., Frisia, S., Hof, F., and Müller, W.: North At-  
lantic storm track changes during the Last Glacial Maximum recorded by Alpine speleothems, *Nature Communications*, 6, 6344,  
432 <https://doi.org/10.1038/ncomms7344>, 2015.
- Mahowald, N. M., Muhs, D. R., Levis, S., Rasch, P. J., Yoshioka, M., Zender, C. S., and Luo, C.: Change in atmospheric mineral aerosols  
434 in response to climate: Last glacial period, preindustrial, modern, and doubled carbon dioxide climates, *J. of Geophysical Research:*  
*Atmospheres*, 111, <http://dx.doi.org/10.1029/2005JD006653>, 2006.
- 436 Monnin, E., Indermühle, A., Dällenbach, A., Flückiger, J., Stauffer, B., Stocker, T. F., Raynaud, D., and Barnola, J.-M.: Atmospheric CO<sub>2</sub>  
Concentrations over the Last Glacial Termination, *Science*, 291, 112–114, <http://science.sciencemag.org/content/291/5501/112>, 2001.
- 438 Peyron, O., Guiot, J., Cheddadi, R., Tarasov, P., Reille, M., de Beaulieu, J.-L., Bottema, S., and Andrieu, V.: Climatic Reconstruction in  
Europe for 18,000 YR B.P. from Pollen Data, *Quaternary Research*, 49, 183–196, <http://dx.doi.org/10.1006/qres.1997.1961>, 1998.
- 440 Prentice, I. C. and Harrison, S. P.: Ecosystem effects of CO<sub>2</sub> concentration: evidence from past climates, *Climate of the Past*, 5, 297–307,  
<http://dx.doi.org/10.5194/cp-5-297-2009>, 2009.
- 442 Renssen, H., Kasse, C., Vandenberghe, J., and Lorenz, S. J.: Weichselian Late Pleniglacial surface winds over northwest and central Europe:  
a model–data comparison, *J. of Quaternary Science*, 22, 281–293, <http://dx.doi.org/10.1002/jqs.1038>, 2007.
- 444 Reyers, M., Pinto, J. G., and Moemken, J.: Statistical-dynamical downscaling for wind energy potentials: evaluation and applications to  
decadal hindcasts and climate change projections, *International J. of Climatology*, 35, 229–244, <https://doi.org/10.1002/joc.3975>, <http://dx.doi.org/10.1002/joc.3975>, 2014.
- 446 Römer, W., Lehmkuhl, F., and Sirocko, F.: Late Pleistocene aeolian dust provenances and wind direction changes reconstructed by heavy  
448 mineral analysis of the sediments of the Dehner dry maar (Eifel, Germany), *Global and Planetary Change*, 147, 25–39, <http://dx.doi.org/10.1016/j.gloplacha.2016.10.012>, 2016.
- 450 Shao, Y.: Simplification of a dust emission scheme and comparison with data, *J. of Geophysical Research*, 109, <http://dx.doi.org/10.1029/2003JD004372>, 2004.
- 452 Shao, Y., Anhäuser, A., Ludwig, P., Schlüter, P., and Williams, E.: Statistical reconstruction of global vegetation for the last glacial maximum,  
*Global and Planetary Change*, 168, 67 – 77, <http://www.sciencedirect.com/science/article/pii/S0921818117306148>, 2018.
- 454 Sima, A., Rousseau, D.-D., Kageyama, M., Ramstein, G., Schulz, M., Balkanski, Y., Antoine, P., Dulac, F., and Hatté, C.: Imprint of North-  
Atlantic abrupt climate changes on western European loess deposits as viewed in a dust emission model, *Quaternary Science Reviews*, 28,  
456 2851–2866, <http://dx.doi.org/10.1016/j.quascirev.2009.07.016>, 2009.
- Sima, A., Kageyama, M., Rousseau, D.-D., Ramstein, G., Balkanski, Y., Antoine, P., and Hatté, C.: Modeling dust emission response to  
458 North Atlantic millennial-scale climate variations from the perspective of East European MIS 3 loess deposits, *Climate of the Past*, 9,  
1385–1402, <https://doi.org/10.5194/cp-9-1385-2013>, <http://dx.doi.org/10.5194/cp-9-1385-2013>, 2013.



- 460 Singhvi, A., Bluszcz, A., Bateman, M., and Rao, M.: Luminescence dating of loess–palaeosol sequences and coversands: methodological aspects and palaeoclimatic implications, *Earth-Science Reviews*, 54, 193–211, [http://dx.doi.org/10.1016/S0012-8252\(01\)00048-4](http://dx.doi.org/10.1016/S0012-8252(01)00048-4), 2001.
- 462 Stevens, B., Giorgetta, M., Esch, M., Mauritsen, T., Crueger, T., Rast, S., Salzmann, M., Schmidt, H., Bader, J., Block, K., Brokopf, R., Fast, I., Kinne, S., Kornblueh, L., Lohmann, U., Pincus, R., Reichler, T., and Roeckner, E.: Atmospheric component of the MPI-M Earth System Model: ECHAM6, *J. of Advances in Modeling Earth Systems*, 5, 146–172, <https://doi.org/10.1002/jame.20015>, 2013.
- 464 Su, L. and Fung, J. C. H.: Sensitivities of WRF-Chem to dust emission schemes and land surface properties in simulating dust cycles during springtime over East Asia, *J. of Geophysical Research: Atmospheres*, 120, 11, <https://doi.org/10.1002/2015JD023446>, 2015.
- 466 Sudarchikova, N., Mikolajewicz, U., Timmreck, C., O’Donnell, D., Schurgers, G., Sein, D., and Zhang, K.: Modelling of mineral dust for interglacial and glacial climate conditions with a focus on Antarctica, *Climate of the Past*, 11, 765–779, <http://dx.doi.org/10.5194/cp-11-765-2015>, 2015.
- 470 Ugan, A. and Byers, D.: Geographic and temporal trends in proboscidean and human radiocarbon histories during the late Pleistocene, *Quaternary Science Reviews*, 26, 3058–3080, <http://dx.doi.org/10.1016/j.quascirev.2007.06.024>, 2007.
- 472 Újvári, G., Stevens, T., Molnár, M., Demény, A., Lambert, F., Varga, G., Jull, A. T., Páll-Gergely, B., Buylaert, J.-P., and Kovács, J.: Coupled European and Greenland last glacial dust activity driven by North Atlantic climate, *Proceedings of the National Academy of Sciences*, 114, E10632–E10638, <https://doi.org/10.1073/pnas.1712651114>, 2017.
- 474 Varga, G., Kovács, J., and Újvári, G.: Late Pleistocene variations of the background aeolian dust concentration in the Carpathian Basin: an estimate using decomposition of grain-size distribution curves of loess deposits, *Netherlands Journal of Geosciences*, 91, 159–171, <http://dx.doi.org/10.1017/S0016774600001566>, 2012.
- 476 Werner, M.: Seasonal and interannual variability of the mineral dust cycle under present and glacial climate conditions, *J. of Geophysical Research*, 107, <http://dx.doi.org/10.1029/2002JD002365>, 2002.
- 478 Wesely, M.: Parameterization of surface resistances to gaseous dry deposition in regional-scale numerical models, *Atmospheric Environment* (1967), 23, 1293–1304, [http://dx.doi.org/10.1016/0004-6981\(89\)90153-4](http://dx.doi.org/10.1016/0004-6981(89)90153-4), 1989.
- 480 Willis, K. and van Andel, T.: Trees or no trees? The environments of central and eastern Europe during the Last Glaciation, *Quaternary Science Reviews*, 23, 2369–2387, <https://doi.org/10.1016/j.quascirev.2004.06.002>, <http://dx.doi.org/10.1016/j.quascirev.2004.06.002>, 2004.
- 482 Yokoyama, Y., Lambeck, K., De Deckker, P., Johnson, P., and Fifield, K.: Timing for the maximum of the Last Glacial constrained by lowest sea-level observations, *Nature*, 406, 713–716, 2000.
- 484 Újvári, G., Kovács, J., Varga, G., Raucsik, B., and Marković, S. B.: Dust flux estimates for the Last Glacial Period in East Central Europe based on terrestrial records of loess deposits: a review, *Quaternary Science Reviews*, 29, 3157–3166, <http://dx.doi.org/10.1016/j.quascirev.2010.07.005>, 2010.
- 488 Újvári, G., Varga, A., Ramos, F. C., Kovács, J., Németh, T., and Stevens, T.: Evaluating the use of clay mineralogy, Sr–Nd isotopes and zircon U–Pb ages in tracking dust provenance: An example from loess of the Carpathian Basin, *Chemical Geology*, 304–305, 83–96, <http://dx.doi.org/10.1016/j.chemgeo.2012.02.007>, 2012.